

# Diphoton plus $Z$ production at the ILC at $\mathcal{O}(\alpha^4)$

Zhang Yu, Guo Lei, Ma Wen-Gan, Zhang Ren-You, Chen Chong, and Li Xiao-Zhou  
Department of Modern Physics, University of Science and Technology of China (USTC),  
Hefei, Anhui 230026, P.R.China

## Abstract

Precision measurement for the production of a  $Z$ -boson in association with two photons is important for investigating Higgs boson and exploring new physics at the International Linear Collider (ILC). It could be used to study the  $ZZ\gamma\gamma$  anomalous quartic gauge coupling. In this work we report on our calculation of the full  $\mathcal{O}(\alpha^4)$  contributions to the  $e^+e^- \rightarrow Z\gamma\gamma$  process in the standard model, and analyze the electroweak (EW) quantum effects on the total cross section. We investigate the dependence of the  $Z\gamma\gamma$  production rate on the event selection scheme and provide distributions for some important kinematic observables. We find that the next-to-leading order (NLO) EW corrections can enhance the total cross section quantitatively from 2.32% to 9.61% when colliding energy goes up from 250  $GeV$  to 1  $TeV$ , and the NLO EW corrections show obviously a non trivial phase space dependence. We conclude that in studying the signal process  $e^+e^- \rightarrow ZH \rightarrow Z\gamma\gamma$ , the background process  $e^+e^- \rightarrow Z\gamma\gamma$  can be suppressed significantly if we take appropriate kinematic cuts on the final products.

PACS: 13.66.-a, 14.70.Hp, 14.70.Bh

## I. Introduction

Probing the mechanism of electroweak symmetry breaking (EWSB) is one of the most important tasks of particle physics. In the standard model (SM) the symmetry breaking is achieved by introducing the Higgs mechanism, which gives mass to massive elementary particles and implies the existence of an SM Higgs boson. Therefore, to uncover the origin of EWSB and to determine whether the SM Higgs boson really exists is one of the highlights of the Large Hadron Collider (LHC) physics programmes [1]. In last July, both ATLAS and CMS collaborations at the LHC reported that they had observed a new neutral boson with mass of around  $126\text{ GeV}$  [2, 3], and this particle is tentatively identified as Higgs boson on this March. The more precise measurements on its properties are still going on at the LHC, but in light of the current data, its properties are very well compatible with the SM Higgs boson. However, it has been understood for a long time that there are intrinsic limitations from the ability of hadron colliders in the precision measurements. The International Linear Collider (ILC) is an ideal machine to address this problem [4]. One of the major aspects of the physics program of the ILC is to give the detailed precision measurements of the nature of the Higgs boson discovered at the LHC [4, 5].

For any observed new particle, the determination of its fundamental property will be a primary goal. The measurement of the branching fraction of the Higgs boson into two photons,  $Br(H \rightarrow \gamma\gamma)$ , turns out to be an absolutely necessary ingredient in extracting the total width [6]. Besides, this measurement may possibly provide hints for new physics if the deviation from the SM prediction is larger than the measurement accuracy. At the ILC the Higgs boson is predominantly produced by the Higgs-strahlung process  $e^+e^- \rightarrow ZH$ . The most serious and irreducible background for Higgs search via  $H \rightarrow \gamma\gamma$  decay channel, arises from the process  $e^+e^- \rightarrow Z\gamma\gamma$  which is hard to be got rid of and needs to be explored in depth [7].

The precision measurements of the quartic gauge-boson coupling (QGC) can provide a connection to the mechanism of electroweak symmetry breaking. The anomalous QGC, such as  $ZZ\gamma\gamma$ , vanishes in the SM at the tree level and might provide a clean signal of new physics, since any deviation from the SM prediction might be connected to the residual effect of electroweak symmetry breaking. The effect of  $ZZ\gamma\gamma$  coupling has been theoretically investigated at the LEP and the ILC [8–13]. The

measurement of the  $e^+e^- \rightarrow Z\gamma\gamma$  process at LEP2 by L3 Collaboration [14] shows that the anomalous  $ZZ\gamma\gamma$  coupling leads to negligible effect at LEP energy, while it might be detectable at the ILC with higher colliding energy. Since this effect can be small and subtle, the theoretical predictions for the cross section with high precision is mandatory.

At the ILC, the accuracy of the cross section measurement for the triple gauge-bosons production process could reach per-mille level, it is necessary to presume upon an accurate theoretical calculations to match the experimental accuracy. Thus a good theoretical predictions beyond leading order (LO) is indispensable. In the last few years, a lot of works contributed to the phenomenological studies in the SM up to the QCD next-to-leading order (NLO) on triple gauge-boson production processes at hadron colliders [15–23]. Most recently, the calculation of the NLO electroweak (EW) correction to the  $W^+W^-Z$  production at the LHC was present in Ref. [24]. The NLO EW calculations to the  $W^+W^-Z$  and  $ZZZ$  productions at the ILC were provided in Refs. [25–27], while the prediction for the  $Z$  production associated with two photons at the ILC in NLO EW precision is still missing.

In this paper, we investigate the complete NLO EW corrections to the  $e^+e^- \rightarrow Z\gamma\gamma$  process at the ILC in the SM. The rest of the paper is organized as follows: In the following section we present the LO and the NLO EW analytical calculations for the  $e^+e^- \rightarrow Z\gamma\gamma$  process. The numerical results and discussions are given in Section III. Finally, we will give a short summary.

## II. Analytical calculations

The LO and NLO EW calculations for the  $e^+e^- \rightarrow Z\gamma\gamma$  process in the SM are presented in this section by using the 't Hooft-Feynman gauge. We apply FeynArts3.7 package [28] to automatically generate the Feynman diagrams, and FormCalc7.2 program [29] to simplify algebraically the corresponding amplitudes. In our calculations we neglect the contributions of the Feynman diagrams which involve  $H$ - $e$ - $\bar{e}$ ,  $G^0$ - $e$ - $\bar{e}$ ,  $G^+$ - $e$ - $\bar{\nu}_e$  or  $G^-$ - $\nu_e$ - $\bar{e}$  vertex, because the Yukawa coupling strength of Higgs/Goldstone to fermions is proportional to the fermion mass.

We denote the process as

$$e^+(p_1) + e^-(p_2) \rightarrow Z(p_3) + \gamma(p_4) + \gamma(p_5), \quad (2.1)$$

where  $p_i$  ( $i = 1, 5$ ) represent the four-momenta of all initial and final particles. The LO Feynman

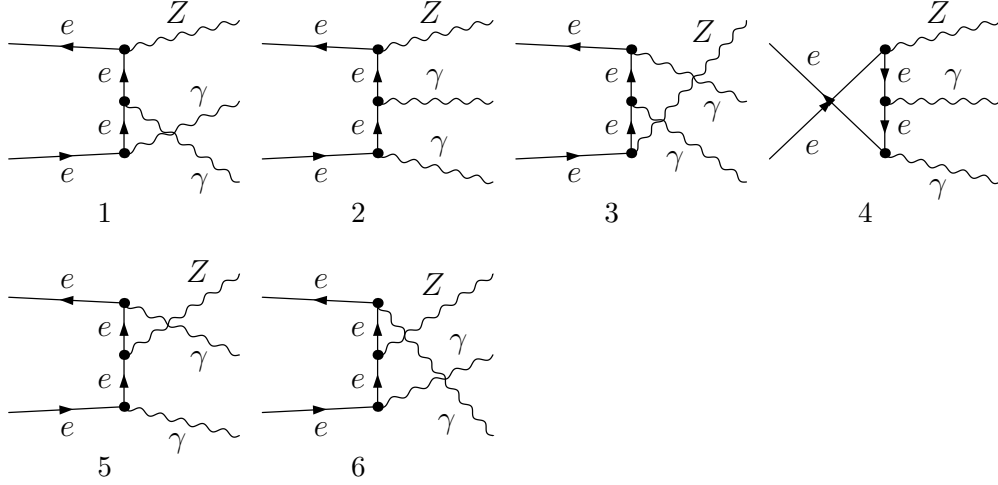


Figure 1: The tree-level Feynman diagrams for the  $e^+e^- \rightarrow Z\gamma\gamma$  process.

diagrams for the process are depicted in Figure 1. The LO cross section for the  $e^+e^- \rightarrow Z\gamma\gamma$  process can be obtained as

$$\sigma_{LO} = \frac{1}{2!} \frac{(2\pi)^4}{2s} \int d\Phi_3 \overline{\sum_{spin}} |\mathcal{M}_{LO}|^2, \quad (2.2)$$

where  $\mathcal{M}_{LO}$  is the amplitude of all the LO diagrams, the factor  $\frac{1}{2!}$  is due to two identical final photons and the bar over summation recalls averaging over initial spins. The phase space element of the final three particles is defined as

$$d\Phi_3 = \delta^{(4)} \left( p_1 + p_2 - \sum_{i=3}^5 p_i \right) \prod_{i=3}^5 \frac{d^3\vec{p}_i}{(2\pi)^3 2E_i}. \quad (2.3)$$

The virtual EW corrections to the  $e^+e^- \rightarrow Z\gamma\gamma$  process at  $\mathcal{O}(\alpha^4)$  involve 1003 diagrams, including 36 self-energy diagrams, 472 triangles, 418 boxes, 47 pentagons, and 30 counterterm graphs. The most complicated topologies involved in the EW one-loop amplitude contain 5-point integral functions up to rank 4, which are deduced by using the reduction method in Ref. [30]. The numerical calculations of  $n$ -point ( $n \leq 4$ ) tensor integrals are implemented by using the Passarino-Veltman reduction algorithm [31]. In order to avoid instability in the numerical calculations of 5-point tensor integrals of rank 4, we use the programs coded in Fortran77 with quadruple precision for the numerical calculation of the pentagons plotted in Fig.2. The virtual EW correction to the  $e^+e^- \rightarrow Z\gamma\gamma$  process can be expressed

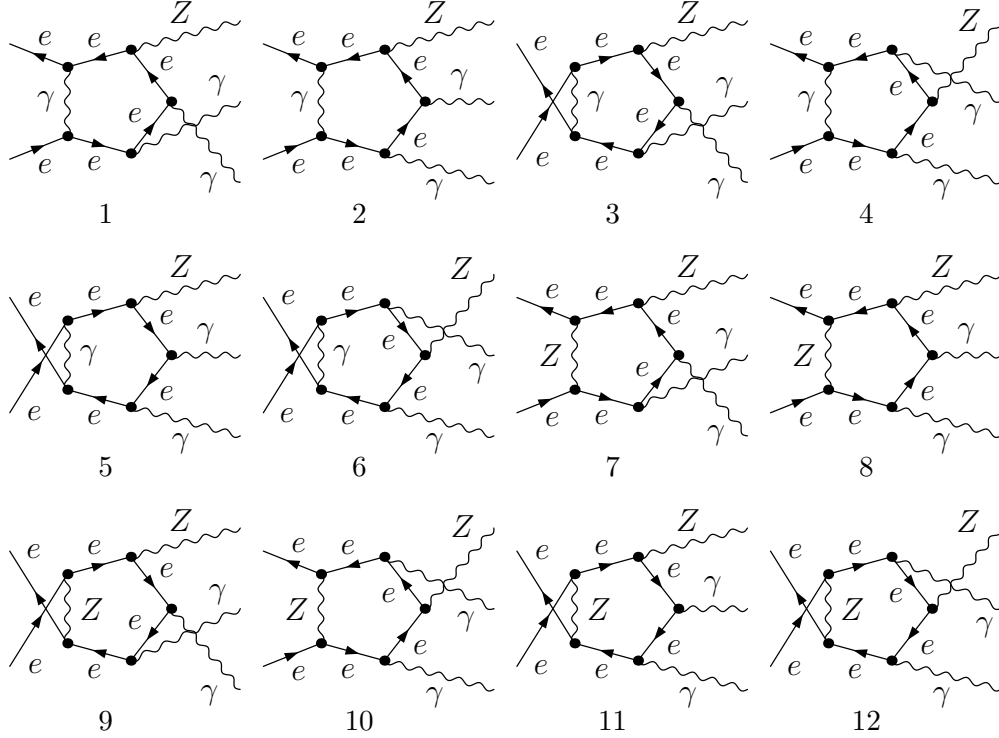


Figure 2: The pentagon diagrams which are calculated by using the codes with quadruple precision for the  $e^+e^- \rightarrow Z\gamma\gamma$  process.

as:

$$\Delta\sigma_v = \frac{1}{2!} \frac{(2\pi)^4}{2s} \int d\Phi_3 \sum_{spin} 2Re \{ \mathcal{M}_v \mathcal{M}_{LO}^* \}, \quad (2.4)$$

where  $\mathcal{M}_v$  is the amplitude for all the virtual Feynman diagrams.

The one-loop Feynman diagrams with possible Higgs or  $Z$ -boson on-shell effects for the  $e^+e^- \rightarrow Z\gamma\gamma$  process are shown in Fig.3. The interference between the amplitude of these two Feynman diagrams and the LO amplitude leads to propagator factors of  $\frac{1}{(M_{\gamma\gamma}^2 - M_Z^2)}$  and  $\frac{1}{(M_{\gamma\gamma}^2 - M_H^2)}$ , which are divergent in the vicinities of  $M_{\gamma\gamma}^2 \sim M_Z^2$  and  $M_{\gamma\gamma}^2 \sim M_H^2$  separately. We regulate them by making the replacements of  $\frac{1}{(M_{\gamma\gamma}^2 - M_Z^2)} \rightarrow \frac{1}{(M_{\gamma\gamma}^2 - M_Z^2 + iM_Z\Gamma_Z)}$  and  $\frac{1}{(M_{\gamma\gamma}^2 - M_H^2)} \rightarrow \frac{1}{(M_{\gamma\gamma}^2 - M_H^2 + iM_H\Gamma_H)}$ , respectively. We find that the contributions of these interference amplitudes are so tiny that can be ignored in the total NLO EW correction.

The amplitude for all the one-loop Feynman diagrams (except for the counterterm diagrams) contains both ultraviolet (UV) and infrared (IR) singularities. We adopt the dimensional regularization scheme [32], in which the dimensions of spinor and space-time manifolds are extend to  $D = 4 - 2\epsilon$ , to

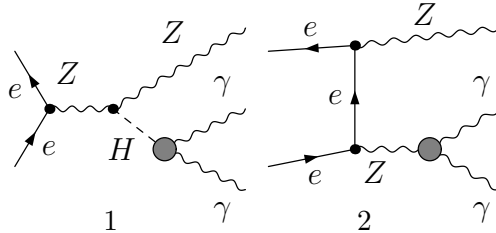


Figure 3: The one-loop diagrams with possible on-shell internal Higgs or  $Z$ -boson for the  $e^+e^- \rightarrow Z\gamma\gamma$  process.

regularize both the UV and the IR divergences in loop integrals. The relevant fields are renormalized by adopting the on-mass-shell (OMS) renormalization scheme and the explicit expressions for the renormalization constants are detailed in Refs. [33, 34]. As we expect, the UV divergence contained in the loop virtual amplitude can be canceled by that in the counterterm amplitude exactly.

In order to get an IR-finite cross section for the  $e^+e^- \rightarrow Z\gamma\gamma$  process at the EW NLO, we consider the real photon emission process  $e^+(p_1) + e^-(p_2) \rightarrow Z(p_3) + \gamma(p_4) + \gamma(p_5) + \gamma(p_6)$ . The contribution of the real photon emission process has the form as

$$\Delta\sigma_{real} = \frac{1}{3!} \frac{(2\pi)^4}{2s} \int d\Phi_4 \sum_{spin} |\mathcal{M}_{real}|^2, \quad (2.5)$$

where  $\frac{1}{3!}$  is due to the three final identical final photons. The phase space element of the four final particles is defined as

$$d\Phi_4 = \delta^{(4)}\left(p_1 + p_2 - \sum_{i=3}^6 p_i\right) \prod_{j=3}^6 \frac{d^3\vec{p}_j}{(2\pi)^3 2E_j}. \quad (2.6)$$

We employ the dipole subtraction method to extract the IR singularity from the real photon emission correction, and combine them with the virtual contribution. In this method, the squared amplitude of the real photon emission process is subtracted by an auxiliary function with the same asymptotic behavior as the LO amplitude squared for the  $Z\gamma\gamma$  production process. Then the IR-finite real correction is obtained before integrating over phase-space. The subtracted term is added again after analytical integration over the bremsstrahlung photon phase space. The dipole subtraction formalism is a process independent approach and was first presented by Catani and Seymour for QCD with massless partons [35, 36] and subsequently generalized to photon radiation off charged particles with arbitrary mass by Dittmaier [37]. In our calculations, we follow the approach of Ref. [37]. The

cancelation of infrared pole from the virtual amplitude with that from the real radiation correction was verified. We also checked the independence on the parameter  $\alpha \in (0, 1]$  which essentially controls the region of phase space over the subtracted terms, such as  $\alpha = 1$  means the full dipole subtraction have been considered, to ensure the real radiation part is correctly calculated [38].

To analyze the origin of the NLO EW corrections clearly, we calculate the photonic (QED) and the genuine weak corrections separately. The QED correction includes two parts: the QED virtual correction  $\Delta\sigma_v^{QED}$  contributed by the loop diagrams with virtual photon exchange in loop and the corresponding counterterm diagrams, and the real photon emission correction  $\Delta\sigma_{real}$ . The rest of the virtual electroweak correction part is called the weak correction  $\Delta\sigma_v^W$ . Therefore, the full NLO EW corrected cross section can be expressed as:

$$\begin{aligned}\sigma_{NLO} &= \sigma_{LO} + \Delta\sigma_v + \Delta\sigma_{real} = \sigma_{LO} + \Delta\sigma_v^{QED} + \Delta\sigma_v^W + \Delta\sigma_{real} \\ &= \sigma_{LO} + \Delta\sigma^{QED} + \Delta\sigma_v^W = \sigma_{LO}(1 + \delta^{QED} + \delta^W) = \sigma_{LO}(1 + \delta^{EW}),\end{aligned}\quad (2.7)$$

where the  $\delta^{QED}$ ,  $\delta^W$  and  $\delta^{EW}$  are the pure QED, genuine weak and full EW relative corrections, respectively.

### III. Numerical results and discussions

#### III.1 Input parameters and kinematic cuts

For the numerical evaluation we adopt the  $\alpha$ -scheme and take the following SM input parameters [39]:

$$\begin{aligned}M_W &= 80.398 \text{ GeV}, & M_Z &= 91.1876 \text{ GeV}, & \Gamma_Z &= 2.4952 \text{ GeV} \\ m_e &= 0.510998929 \text{ MeV}, & m_\mu &= 105.6583715 \text{ MeV}, & m_\tau &= 1.77682 \text{ GeV}, \\ m_u &= 66 \text{ MeV}, & m_c &= 1.275 \text{ GeV}, & m_t &= 173.5 \text{ GeV}, \\ m_d &= 66 \text{ MeV}, & m_s &= 95 \text{ MeV}, & m_b &= 4.65 \text{ GeV}.\end{aligned}\quad (3.1)$$

We take the fine structure constant  $\alpha(0) = 1/137.035999074$  defined in the Thomson limit. The current masses for light quarks ( $m_u$  and  $m_d$ ) can reproduce the hadronic contribution to the shift in the fine structure constant  $\alpha(M_Z)$  [40]. We take the Higgs boson mass as  $M_H = 126 \text{ GeV}$  and its decay width is estimated by using the HDECAY program [41]. The CKM matrix, whose matrix element appears only in loop, is set to be unity matrix.

We apply the Cambridge/Aachen (C/A) jet algorithm [42] to photon candidates. For three-photon event originating from the real emission correction, when two final photons with the smallest separation

$R$  in the three-photon event satisfy the constraint of  $R = \sqrt{\Delta y^2 + \Delta\phi^2} < 0.4$ , where  $\Delta y$  and  $\Delta\phi$  are the differences of rapidity and azimuthal angle between the two photons, we combine this pair of photons as one new photon track and the event is considered as a two-photon event including the merged photon with four-momentum  $p_{ij,\mu} = p_{i,\mu} + p_{j,\mu}$ , and contrariwise, it is considered as a three-photon event. We name the photon with the largest transverse energy as the leading photon, while the photon with the next largest transverse energy is called subleading photon. We take the cuts on all final photons for both the two-photon event and three-photon event as

$$p_T^\gamma \geq 15 \text{ GeV}, \quad |y_\gamma| \leq 2.5, \quad R_{\gamma\gamma} \geq 0.4. \quad (3.2)$$

Thereby we exclude the inevitably infrared (IR) singularity at the tree level. In the 'inclusive' scheme we include all the two- and three-photon events which satisfy the cuts of Eq.(3.2). In the 'exclusive' event selection scheme, we collect only the so-called two-photon events and apply the constraints as shown in Eq.(3.2) on final two photons. In following we apply the 'inclusive' scheme for event selection as default unless stated otherwise.

### III.2 Total cross section

The dependence of the LO integrated cross section for the  $e^+e^- \rightarrow Z\gamma\gamma$  process in the SM on the colliding energy was presented in Fig.1 of Ref. [10]. When we take the same input parameters as in that reference, the coincident numerical results can be obtained. In Fig.4(a), we plot the LO, NLO EW and pure NLO QED corrected integrated cross sections as the functions of the colliding energy  $\sqrt{s}$  in the 'inclusive' event selection scheme, and the corresponding NLO EW and pure NLO QED relative corrections,  $\delta^{EW} \equiv \frac{\sigma_{NLO} - \sigma_{LO}}{\sigma_{LO}}$  and  $\delta^{QED} \equiv \frac{\sigma_{NLO}^{QED} - \sigma_{LO}}{\sigma_{LO}}$ , are illustrated in Fig.4(b). Some representative numerical results read out from Figs.4(a) and (b) are listed in Table 1. From these figures we find all the curves for the cross sections decrease quickly with the increment of  $\sqrt{s}$ , and the LO cross section is always enhanced by the NLO EW corrections in the whole  $\sqrt{s}$  plotted range. When  $\sqrt{s}$  goes up from 250 GeV to 1 TeV, the NLO EW relative correction  $\delta^{EW}$  varies from 2.32% to 9.61%. We also see that the pure NLO QED correction part always increases the LO cross section when  $\sqrt{s} > 270 \text{ GeV}$  and the pure NLO QED relative correction becomes more and more notable with the increment of  $\sqrt{s}$ . In order to make a comparison of the results by adopting different event selection schemes, we also



$\sqrt{s}(GeV)$	$\sigma_{LO}(fb)$	$\sigma_{NLO}(fb)$	$\sigma_{NLO}^{QED}(fb)$	$\delta^{EW}(\%)$	$\delta^{QED}(\%)$
250	159.05(4)	162.73(13)	157.39(18)	2.32	-1.04
300	133.41(4)	139.71(12)	135.79(17)	4.72	1.79
400	93.12(3)	99.61(7)	97.65(9)	6.97	4.86
500	68.74(2)	74.25(4)	73.40(5)	8.02	6.77
600	53.18(2)	57.76(5)	57.54(7)	8.61	8.20
700	42.62(1)	46.46(3)	46.63(4)	9.00	9.42
800	35.07(1)	38.32(3)	38.75(3)	9.27	10.48
900	29.47(1)	32.25(3)	32.84(3)	9.42	11.42
1000	25.12(1)	27.53(3)	28.23(3)	9.61	12.39

Table 1: The total LO, NLO EW, pure NLO QED corrected integrated cross sections ( $\sigma_{LO}$ ,  $\sigma_{NLO}$  and  $\sigma_{NLO}^{QED}$ ), and the corresponding EW and QED relative corrections ( $\delta^{EW}$  and  $\delta^{QED}$ ) for the  $e^+e^- \rightarrow Z\gamma\gamma$  process in the 'inclusive' event selection scheme.

$\sqrt{s}(GeV)$	$\sigma_{LO}(fb)$	$\sigma_{NLO}(fb)$	$\sigma_{NLO}^{QED}(fb)$	$\delta^{EW}(\%)$	$\delta^{QED}(\%)$
250	159.05(4)	161.81(13)	156.47(14)	1.74	-1.62
300	133.41(4)	138.56(12)	134.64(12)	3.86	0.92
400	93.12(3)	98.39(7)	96.43(9)	5.66	3.55
500	68.74(2)	73.12(4)	72.26(5)	6.37	5.12
600	53.18(2)	56.74(5)	56.52(7)	6.69	6.28
700	42.62(1)	45.53(3)	45.71(4)	6.83	7.24
800	35.07(1)	37.48(3)	37.91(3)	6.88	8.09
900	29.47(1)	31.49(3)	32.08(3)	6.85	8.85
1000	25.12(1)	26.85(3)	27.54(3)	6.87	9.64

Table 2: The total LO cross section ( $\sigma_{LO}$ ), NLO EW, pure NLO QED corrected integrated cross sections ( $\sigma_{NLO}$  and  $\sigma_{NLO}^{QED}$ ), and the corresponding EW and QED relative corrections ( $\delta^{EW}$  and  $\delta^{QED}$ ) for the  $e^+e^- \rightarrow Z\gamma\gamma$  process in the 'exclusive' event selection scheme.

present corresponding numerical results by adopting the 'exclusive' event selection scheme in Table 2. We find that with the same  $\sqrt{s}$  the NLO EW and pure NLO QED corrected cross sections in Table 2 are normally less than the corresponding ones by adopting the 'inclusive' event selection scheme, due to that three-photon events are abandoned in the 'exclusive' event selection scheme.

### III.3 Kinematic distributions

We present the LO and NLO EW corrected transverse momentum and rapidity distributions of final  $Z$ -boson in Fig.5(a) and Fig.6(a), respectively. The corresponding EW relative corrections  $\delta^{EW}$  are also plotted in Fig.5(b) and Fig.6(b), separately. There the results are obtained by taking  $\sqrt{s} = 500 GeV$  and applying the 'inclusive' event selection scheme. From Fig.5 we can see that the NLO EW correction enhances the LO differential cross section  $d\sigma_{LO}/dp_T^Z$  in low  $p_T^Z$  region. The NLO relative correction

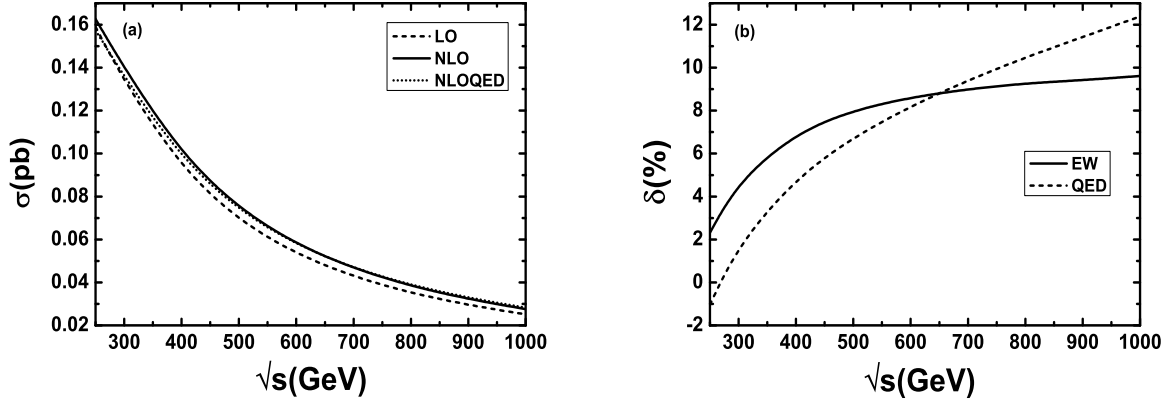


Figure 4: (a) The LO, NLO EW and pure NLO QED corrected cross sections ( $\sigma_{LO}$ ,  $\sigma_{NLO}$ ,  $\sigma_{NLO}^{QED}$ ) for the  $e^+e^- \rightarrow Z\gamma\gamma$  process as the functions of the colliding energy  $\sqrt{s}$  in the 'inclusive' event selection scheme at the ILC. (b) The corresponding NLO EW and pure NLO QED relative corrections ( $\delta^{EW}$ ,  $\delta^{QED}$ ).

always goes down with the increment of  $p_T^Z$ , and changes from positive to negative when  $p_T^Z$  arrives at about 145 GeV. In Figs.6(a,b), we find that LO rapidity distribution is strengthened obviously by NLO EW correction in the central rapidity region of  $Z$ -boson at the ILC, while weakened by the quantum correction in the regions of  $|y_Z| \geq 1.4$ .

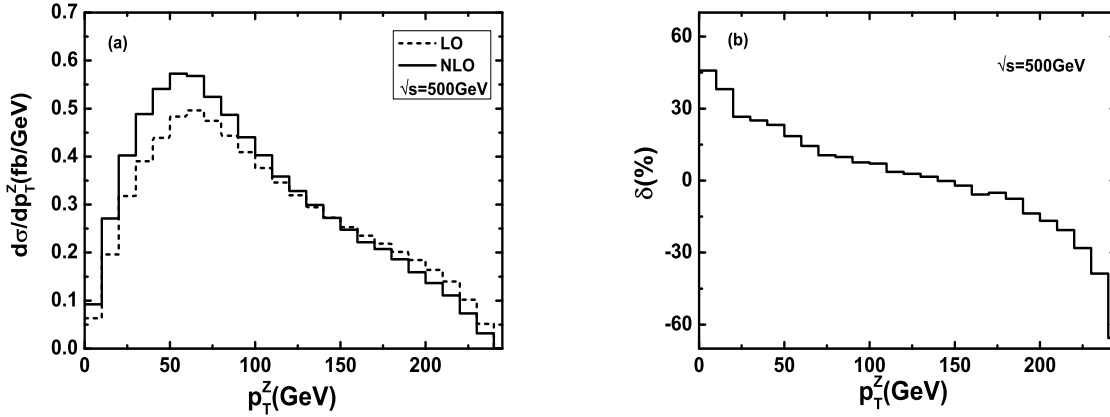


Figure 5: (a) The LO and NLO EW corrected transverse momentum distributions of  $Z$ -boson with  $\sqrt{s} = 500$  GeV in the 'inclusive' event selection scheme. (b) The corresponding NLO EW relative corrections.

The transverse momentum distributions of the leading photon (labeled by  $\gamma_1$ ) and the subleading photon (labeled by  $\gamma_2$ ) are plotted in Fig.7(a) and Fig.7(b), respectively. The rapidity distributions of the leading and subleading photons are presented in Fig.8(a) and Fig.8(b), separately. In these four

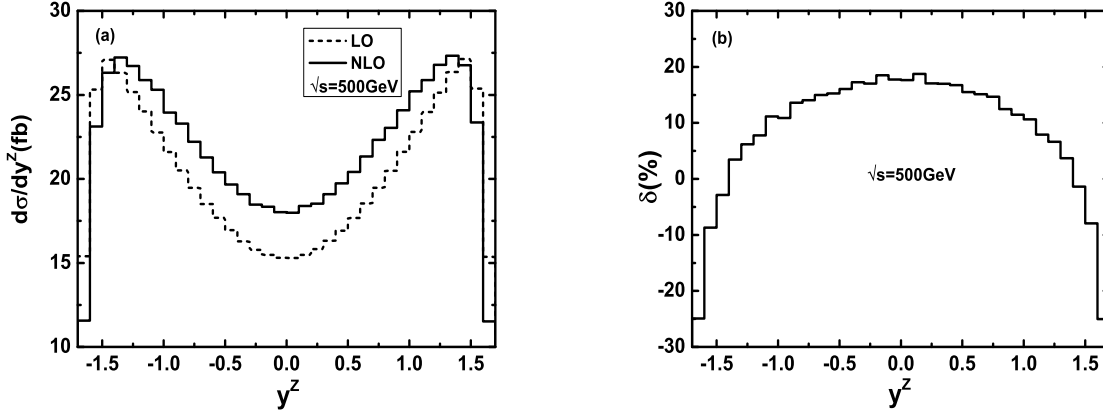


Figure 6: (a) The LO and NLO EW corrected rapidity distributions of  $Z$ -boson with  $\sqrt{s} = 500 \text{ GeV}$  in the 'inclusive' event selection scheme. (b) The corresponding NLO EW relative corrections.

figures we adopt the 'inclusive' event selection scheme, and take  $\sqrt{s} = 500 \text{ GeV}$ , the cuts on photons being declared above. It can be seen from both Figs.7(a) and (b) that the LO  $p_T$  distributions for the leading and subleading photons are enhanced in the lower  $p_T$  region (i.e.,  $p_T^{\gamma_1} < 145 \text{ GeV}$  and  $p_T^{\gamma_2} < 75 \text{ GeV}$ , separately), but suppressed in the rest  $p_T$  regions by the NLO corrections. The LO and NLO EW corrected transverse momentum distributions for the leading photon reach their maxima at about  $50 \text{ GeV}$ . While for the subleading photon, the LO and NLO EW corrected transverse momentum distributions always decrease with the increment of  $p_T$ . Fig.8 shows that the rapidity distributions of the leading and subleading photons are both reinforced by the NLO EW corrections in the whole plotted rapidity region. The figures show that both the LO and NLO corrected rapidity distributions for the leading photon have two peaks, which are located at the positions of  $|y| \sim 1$ , but in contrast the subleading photon rapidity distributions reach their maxima in the central rapidity region.

The LO and NLO EW corrected distributions of the separation  $R_{\gamma\gamma}$  between the final leading and subleading photons are plotted in Fig.9(a). It shows that the preferred kinematical configurations at both the LO and the NLO between the leading and subleading photons are obviously separated with each other in the rapidity- azimuthal-angle plane, and the LO and NLO  $R_{\gamma\gamma}$  distributions reach their maxima at the location of  $R_{\gamma\gamma} \sim 3$ . In Fig.9(b), we depict the LO and NLO EW corrected distributions of the invariant mass of the leading and subleading photons (denoted as  $M_{\gamma\gamma}$ ). It

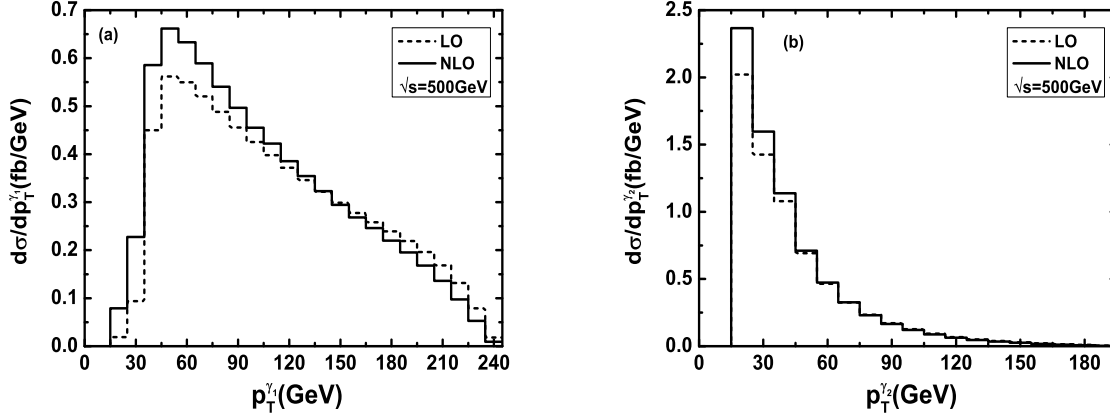


Figure 7: The LO and NLO EW corrected transverse momentum distributions of final photons with  $\sqrt{s} = 500 \text{ GeV}$  in the 'inclusive' event selection scheme. (a) For the leading photon. (b) For the subleading photon.

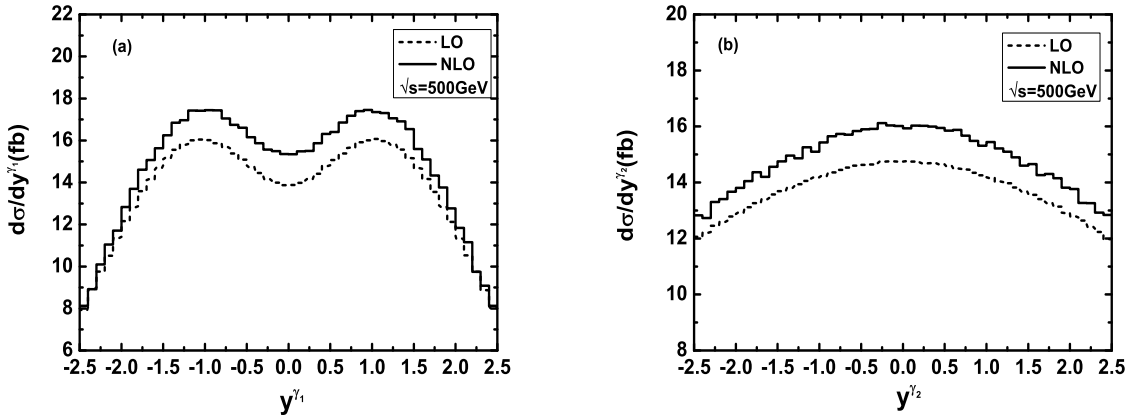


Figure 8: The LO and NLO EW corrected rapidity distributions of final photons with  $\sqrt{s} = 500 \text{ GeV}$  in the 'inclusive' event selection scheme. (a) For the leading photon. (b) For the subleading photon.

demonstrates that both the LO and NLO EW corrected  $M_{\gamma\gamma}$  distributions reach their maxima in the vicinity of  $M_{\gamma\gamma} \sim 100 \text{ GeV}$ , and the NLO EW correction enhances the LO differential cross section when  $M_{\gamma\gamma} \leq 270 \text{ GeV}$ .

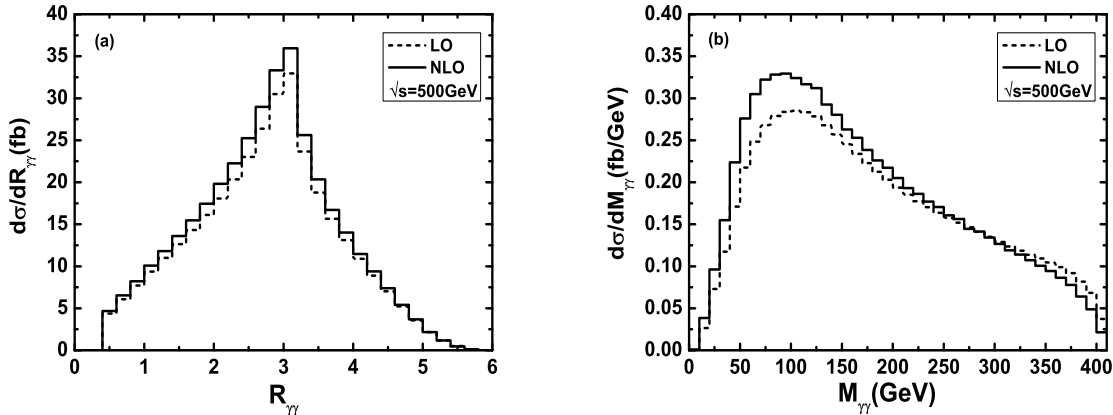


Figure 9: (a) The LO and NLO EW corrected distributions of the separation  $R_{\gamma\gamma}$  between the final leading and subleading photons. (b) The LO and NLO EW corrected invariant mass  $M_{\gamma\gamma}$  distributions.

From the figures of Figs.5-9 we can see that the phase space dependence of the NLO EW correction is non trivial and sizable, and the NLO EW correction does not observably change the LO distribution line shape in case of taking the 'inclusive' event selection scheme.

As we know that one of the most important reaction at the ILC for Higgs boson precision study is the  $e^+e^- \rightarrow ZH$  process followed by  $H \rightarrow \gamma\gamma$  decay, while this signal process is accompanied by a serious background process  $e^+e^- \rightarrow Z\gamma\gamma$ . The one-loop radiative corrections to this signal process within the SM were calculated by A. Denner, *et al* [43]. Here we follow the strategy used in Ref. [43] for the calculation of the  $e^+e^- \rightarrow ZH$  process up to the EW NLO within the SM, and adopt the input parameters presented in our work (see Section III.1) to calculate the LO and NLO EW corrected results for the  $e^+e^- \rightarrow ZH \rightarrow Z\gamma\gamma$  signal process. The decay width of the SM Higgs is obtained by using the program HDECAY [41]. Since the kinematics of the signal events is distinctively different from that of background events. These differences can be used to suppress the background and enhance the ratio of signal to background (S/B). Taking advantage of the kinematic differences, we expect that we can impose the optimal cuts to extract the signal  $e^+e^- \rightarrow ZH \rightarrow Z\gamma\gamma$  from the SM background  $e^+e^- \rightarrow Z\gamma\gamma$  efficiently. For illustration, we present the normalized LO

and NLO EW corrected distributions of various kinematic observables of final particles for the signal process  $e^+e^- \rightarrow ZH \rightarrow Z\gamma\gamma$  and the background process  $e^+e^- \rightarrow Z\gamma\gamma$  in Figs.10(a-f) to demonstrate the distribution differences between the signal and the background. All the results are presented in conditions of  $\sqrt{s} = 500 \text{ GeV}$ ,  $p_T^\gamma \geq 15 \text{ GeV}$ ,  $|y_\gamma| \leq 2.5$ ,  $R_{\gamma\gamma} \geq 0.4$ , and the 'inclusive' event selection scheme. We show the  $p_T$  distributions of final  $Z$ -boson, leading photon and the subleading photon in Figs.10(a-c), separately. We can see that, compared to the background, the typical feature of the signal is that the final state particles are more energetic, especially for the final  $Z$ -boson and the leading photon in the large transverse momentum regions. The normalized rapidity distributions of final leading and subleading photons are demonstrated in Fig.10(d) and Fig.10(e), respectively. It is shown that the leading and subleading photons from Higgs boson decay, mainly appear in the central rapidity region, while the corresponding distributions for background process are rather flat. We can see also from Fig.10(f) that, the leading and subleading photons produced in the background are more dramatically separated than in the signal process  $e^+e^- \rightarrow ZH \rightarrow Z\gamma\gamma$ . From all the figures in Figs.10(a-f), we can see that if we take some proper cuts on kinematic variables of final  $Z$ -boson and photons, the background from the  $e^+e^- \rightarrow Z\gamma\gamma$  process can be significantly suppressed.

## IV. Summary

The  $e^+e^- \rightarrow Z\gamma\gamma$  process is very important for understanding the nature of the Higgs boson and searching for new physics beyond the SM. In this work we report on our calculation of the full NLO EW contributions to the  $e^+e^- \rightarrow Z\gamma\gamma$  process in the SM, and analyze the EW quantum effects on the total cross section and the kinematic distributions of final particles. We study the dependence of the  $Z\gamma\gamma$  production rate on the event selection scheme and provide distributions of some important observables. We find that the full NLO EW corrections can enhance the LO total cross sections quantitatively from 2.32% to 9.61% when colliding energy goes up from 250  $\text{GeV}$  to 1  $\text{TeV}$ , and the size of the NLO correction exhibits a strong dependence on the observable and on phase space. We conclude that in studying the signal process  $e^+e^- \rightarrow ZH \rightarrow Z\gamma\gamma$ , the background events of  $e^+e^- \rightarrow Z\gamma\gamma$  process can be suppressed significantly if we take appropriate kinematic cuts on the final products.

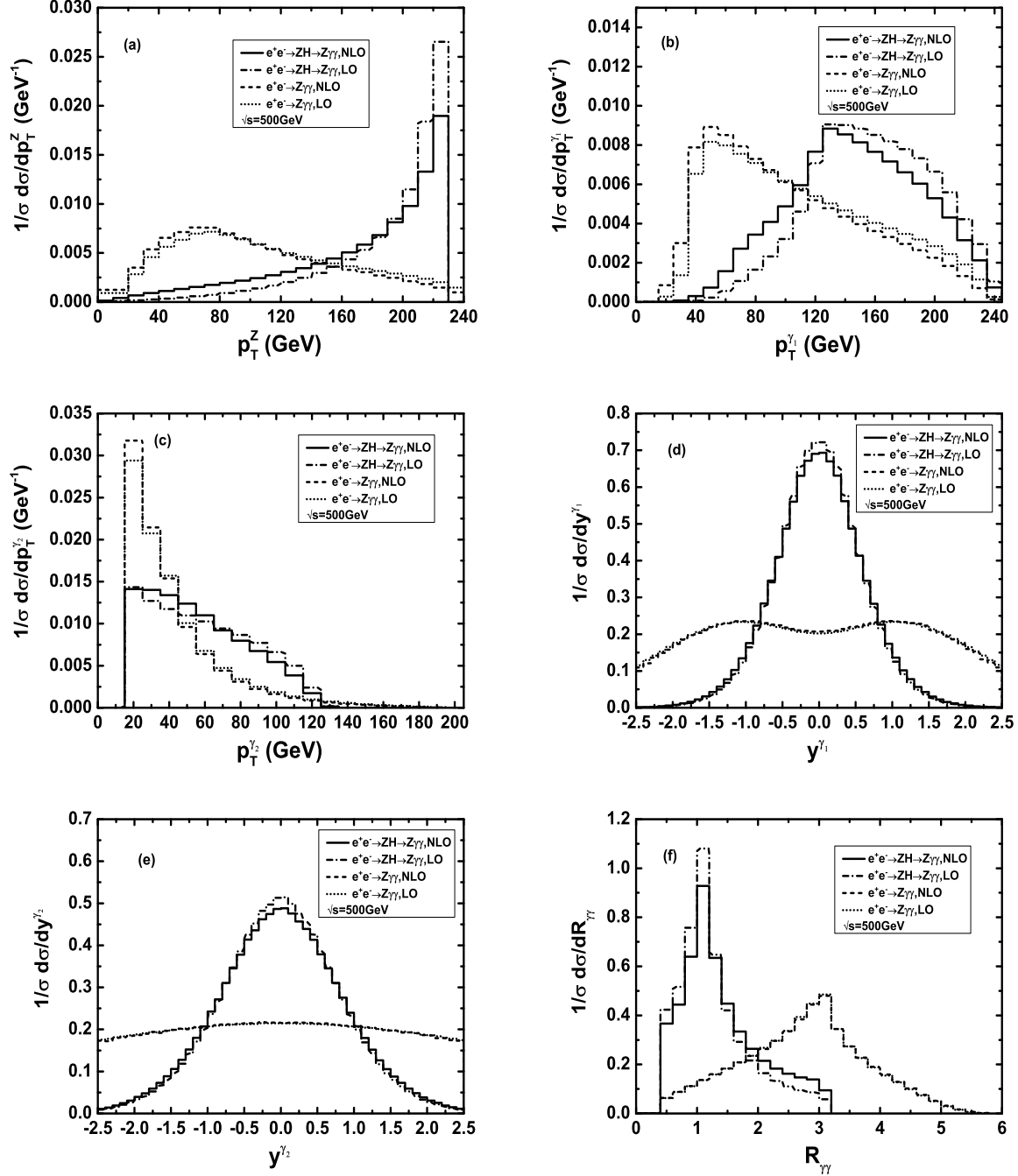


Figure 10: The normalized kinematic distributions for the signal process  $e^+e^- \rightarrow ZH \rightarrow Z\gamma\gamma$  and the background  $e^+e^- \rightarrow Z\gamma\gamma$  process at the  $\sqrt{s} = 500$  GeV ILC. All curves in the six figures are normalized by their total cross sections. (a) Transverse momentum distributions of final  $Z$  boson. (b) Transverse momentum distributions of the leading photon. (c) Transverse momentum distributions of the subleading photon. (d) Rapidity distributions of the leading photon. (e) Rapidity distributions of the subleading photon. (f) Distributions of the separation  $R_{\gamma\gamma}$  between the final leading and subleading photons.

**Acknowledgments:** This work was supported in part by the National Natural Science Foundation of China (Grants. No.11075150, No.11005101, No.11275190), and the Fundamental Research Funds for the Central Universities (Grant. No.WK2030040024).

## References

- [1] L. Evans and P. Bryant (Eds.), LHC Machine, JINST 3 (2008) S08001.
- [2] **CMS** Collaboration, S. Chatrchyan et al., Phys. Lett. **B716**, 30 (2012).
- [3] **ATLAS** Collaboration, G. Aad et al., Phys. Lett. **B716**, 1 (2012).
- [4] H. Baer, et al., 'The International Linear Collider Technical Design Report -Volume 2: Physics', arXiv:1306.6352 [hep-ph].
- [5] D.M. Asner, et al., 'ILC Higgs White Paper', arXiv:1310.0763 [hep-ph].
- [6] John F. Gunion and Patrick C. Martin, Phys. Rev. Lett. **78**, 4541 (1997).
- [7] E. Boos, J.-C. Brient, D.W. Reid, H.J. Schreiber, R. Shadidze, Eur.Phys.J. **C19** 455 (2001).
- [8] G. Belanger and F. Boudjema, Phys. Lett. **B288** 201 (1992).
- [9] G. Belanger and F. Boudjema, Y. Kurihara, D. Perret-Gallix and A. Semenov, Eur.Phys.J. **C13**, 283 (2000).
- [10] W. James Stirling and Anja Werthenbach, Eur.Phys.J. **C14** 103 (2000).
- [11] W. James Stirling and Anja Werthenbach, Phys. Lett. **B466**, 369 (1999).
- [12] G. Montagna, M. Moretti, O. Nicosini, M. Osimo and F. Piccinini, Phys. Lett. **B515** 197 (2001).
- [13] S. Villa, Nucl.Phys.Proc.Suppl. **142**, 391 (2005).
- [14] The L3 Collaboration, P. Achard et al., Phys. Lett. **B540**, 43 (2002).
- [15] A. Lazopoulos, K. Melnikov and F. Petriello, Phys. Rev. **D76**, 014001 (2007).
- [16] V. Hankele and D. Zeppenfeld, Phys. Lett. **B661**, 103 (2008).



- [17] F. Campanario, V. Hankele, C. Oleari, S. Prestel and D. Zeppenfeld, Phys. Rev. **D78**, 094012 (2008).
- [18] T. Binoth, G. Ossola, C. G. Papadopoulos and R. Pittau, JHEP **0806**, 082 (2008).
- [19] G. Bozzi, F. Campanario, V. Hankele and D. Zeppenfeld, Phys. Rev. **D81**, 094030 (2010).
- [20] G. Bozzi, F. Campanario, M. Rauch, H. Rzehak, D. Zeppenfeld, Phys. Lett. **B696**, 380-385 (2011).
- [21] U. Baur, D. Wackerroth and M. M. Weber, PoS **RADCOR2009**, 067 (2010).
- [22] G. Bozzi, F. Campanario, M. Rauch, D. Zeppenfeld. Phys. Rev. **D83**, 114035 (2011).
- [23] G. Bozzi, F. Campanario, M. Rauch, D. Zeppenfeld, Phys. Rev. **D84**, 074028 (2011).
- [24] Dao Thi Nhung, LE Duc Ninh, Marcus M. Weber, 'NLO corrections to WWZ production at the LHC', arXiv:1307.7403.
- [25] J.-J. Su, W.-G. Ma, R.-Y. Zhang, S.-M. Wang, L. Guo, Phys. Rev. **D78**, 016007 (2008).
- [26] W. Sun, W.-G. Ma, R.-Y. Zhang, L. Guo, M. Song, Phys. Lett. **B680**, 321 (2009).
- [27] Fawzi Boudjema, Le Duc Ninh, Sun Hao, Marcus M. Weber, Phys. Rev. **D81**, 073007 (2010).
- [28] T. Hahn, Comput. Phys. Commun. **140**, 418 (2001).
- [29] T. Hahn, M. Perez-Victoria, Comput. Phys. Commun. **118**,(1999) 153.
- [30] A. Denner and S. Dittmaier, Nucl. Phys. **B658**, 175 (2003).
- [31] G. Passarino and M. Veltman, Nucl. Phys. **B160**, 151 (1979).
- [32] G.'t Hooft and M. Veltman, Nucl. Phys. **B44**, 189 (1972).
- [33] D. A. Ross and J. C. Taylor, Nucl. Phys. **B51**, 125 (1973).
- [34] A. Denner, Fortschr.Phys. **41**, 307 (1993).
- [35] S. Catani and M. H. Seymour, Phys. Lett. **B378**, 287 (1996).

- [36] S. Catani, M. H. Seymour, Nucl. Phys. **B485**, 291 (1997); Erratum-ibid. **B510** 503 (1998).
- [37] S. Dittmaier, Nucl. Phys. **B565**, 69 (2000).
- [38] Zoltan Nagy, Zoltan Trocsanyi, Phys. Rev. **D59**, 014020 (1999); Erratum-ibid. **D62**, 099902 (2000); Zoltan Nagy, Phys. Rev. **D68**, 094002 (2003).
- [39] J. Beringer et al. (Particle Data Group), Phys. Rev. **D86**, 010001 (2012).
- [40] F. Jegerlehner, Report No. DESY 01-029, arxiv:hep-ph/0105283.
- [41] A. Djouadi, J. Kalinowski, M. Spira, Comput. Phys. Commun. **108** 56 (1998).
- [42] Gavin P. Salam, Eur. Phys. J. **C67** 637 (2010).
- [43] A. Denner, J. Küblbeck, R. Mertig, M. Böhm Zeit. Phys. C- Particles and Fields **56**, 261-272 (1992).